American Mineralogist, Volume 92, pages 675–686, 2007

Symmetry and crystal structure of biaxial elbaite-liddicoatite tourmaline from the Transbaikalia region, Russia

Alexander Shtukenberg,[1,*] Ira Rozhdestvenskaya,[1] Olga Frank-Kamenetskaya,[1] Julia Bronzova,[1] Harald Euler,[2] Armin Kirfel,[2] Irina Bannova,[1] and Anatoly Zolotarev[3]

[1]Department of Crystallography, Geological Faculty, St. Petersburg State University, Universitetskaya Embankment, 7/9, 199034 St. Petersburg, Russia
[2]Mineralogisch-Petrologisches Institut, Universität Bonn, Poppelsdorfer Schloss, D-53115 Bonn, Germany
[3]Department of Mineralogy, Geological Faculty, St. Petersburg State University, Universitetskaya Embankment, 7/9, 199034 St. Petersburg, Russia

Abstract

Optical anomalies and crystal structures have been studied for an elbaite-liddicoatite tourmaline specimen from the Malkhan pegmatite field (Transbaikalia region, Russia). The specimen is characterized by a complicated zoning and sector zoning distribution of anomalous biaxiality, with the axial angle 2*V* increasing from 3 up to 23° going from the first to the last growth zones of the most developed growth sector, o{02$\bar{2}$1}. The crystal structures of three samples cut out from different growth zones of that sector and characterized by the axial angles 11, 16, and 23° were refined in the trigonal space group *R*3*m* as well as in its monoclinic and triclinic subgroups *Cm*, *R*1, and *P*1, respectively (R = 0.019–0.039). The final choice of the low symmetry space group *R*1 is based on the analysis of the diffraction patterns and on the results of crystal structures refinements, which revealed ordered Al/Li distributions over the Y octahedral sites. The degree of order at Y sites correlates with the axial angle 2*V*, which implies a causal relationship. The Al/Li ordering reflects the geometrical differences of the octahedral sites with respect to the growth front orientation. The results obtained suggest that a growth dissymmetrization mechanism is the main reason for the observed cation ordering and optical anomalies.

Keywords: Optical anomalies, tourmaline crystal structure, elbaite, liddicoatite, growth ordering of atoms, dissymmetrization

Introduction

Since the 19th century natural polychrome tourmalines have been well known for their anomalous optical properties (Brauns 1891). The nominally uniaxial crystals (trigonal space group *R*3*m*) often exhibit biaxiality with the axial angle attaining values of 5–10° or even 30° (Foord and Cunningham 1978; Foord and Mills 1978; Gorskaya et al. 1992; Akizuki et al. 2001). There are two main known reasons for optical anomalies in crystalline solid solutions: (1) internal stress arising from a compositional inhomogeneity of the crystal (e.g., Gorskaya et al. 1992; Shtukenberg et al. 2001) and (2) kinetic ordering of atoms as a growth dissymmetrization phenomenon related to the selective attachment of isomorphous atoms to sites, which are symmetrically equivalent in the bulk crystal but non-equivalent at the crystal surface (e.g., Bulka et al. 1980; Kahr and McBride 1992; Shtukenberg et al. 2005). Both mechanisms can be present in tourmaline and have been cited to explain the observed biaxiality (Foord and Cunningham 1978; Foord and Mills 1978; Gorskaya et al. 1992; Akizuki et al. 2001).

Usually, natural polychrome tourmalines are characterized by relative small optical axial angles and exhibit mainly stress induced optical anomalies (Foord and Mills 1978; Gorskaya et al. 1992). However, as shown by Akizuki et al. (2001), crystals of the elbaite-liddicoatite composition can reveal strong biaxiality (the axial angle attains values up to 30°) supporting that growth ordering of atoms is the most probable reason for the tourmaline biaxiality.

The main objective of the present contribution is to study by means of single-crystal X-ray diffraction the symmetry and crystal structures in sectors of an elbaite-liddicoatite tourmaline exhibiting a strong biaxiality and hence to obtain new information on the origin of the anomalous optical properties of natural tourmaline.

Experimental methods

The investigated tourmaline specimen from the Malkhan pegmatite field (Transbaikalia region, Russia) is pink and about 2 cm long and 0.5–1 cm in diameter. The crystal has a prismatic habit and consists of growth sectors of prisms (m{10$\bar{1}$0} and a{11$\bar{2}$0}) and pyramids (o{02$\bar{2}$1} and r{10$\bar{1}$1}). The crystal was cut into six sections normal to the [0001] direction, which were then inspected with polarized light. The value of the axial angle was measured by Mallard's method with a precision of 0.5°.

The chemical composition was determined by electron probe microanalysis (EPMA) (Camebax SX-50). The following standards have been used: hornblende for Si, Al, Ca, Fe, albite for Na, synthetic "fluorphlogopite" for F, pyrophanite for Mn and Ti. The chemical formula was calculated on the basis of six Si atoms assuming the idealized chemical composition $(Ca,Na,\square)(Al,Li,Mn,Fe,Ti)_3Al_6(Si_6O_{18})(BO_3)_3(O,OH)_3(OH,F)$. The Li content was deduced assuming full occupancy of the octahedral sites, and the O and OH contents were calculated from the charge balance.

To perform crystal structure refinements, three tourmaline samples with significantly different 2*V* values (S1, S5, and S6) were cut from different sections of

* E-mail: sasha@as3607.spb.edu

the growth sector o{02$\bar{2}$1} (Table 1, Fig. 1). These samples were shaped to spheres using an air grinder. For the samples S1 and S6, room-temperature diffraction data were collected on an X-ray Bruker AXS Kappa X8 APEX II autodiffractometer (Mo$K\alpha$ radiation, graphite monochromator) equipped with a CCD-detector (see Table 1 for the experimental details). The sample S5 was studied on a Nicolet-P3/R3 autodiffractometer (Mo$K\alpha$ radiation, graphite monochromator) equipped with a conventional scintillation counter. For all samples, reflections were measured in the full sphere up to the $2\Theta_{max}$ angles specified in Table 1. The measured reflection intensities were then corrected for long-term fluctuations of the incident beam. Absorption corrections for the spherical samples were carried out with the MULTISCAN program (Blessing 1995). To obtain more accurate lattice constants the samples S1 and S6 were additionally studied on a four-circle diffractometer RIGAKU, AFC6R (rotating anode, Mo$K\alpha$ radiation, graphite monochromator) also equipped with a conventional scintillation counter. The refinements of the respective crystal structures were performed with the SHELXL program package (Sheldrick 1997) using neutral atom scattering factors, anomalous dispersion corrections f', f'' and absorption coefficients taken from the *International Tables for Crystallography* (Wilson 1992) and applying the weighting schemes recommended by SHELXL. Along with the atomic coordinates, anisotropic displacement parameters and occupancies an extinction parameter was refined in the standard form used by SHELXL. The initial atomic coordinates were taken from (Gorskaya et al. 1982).

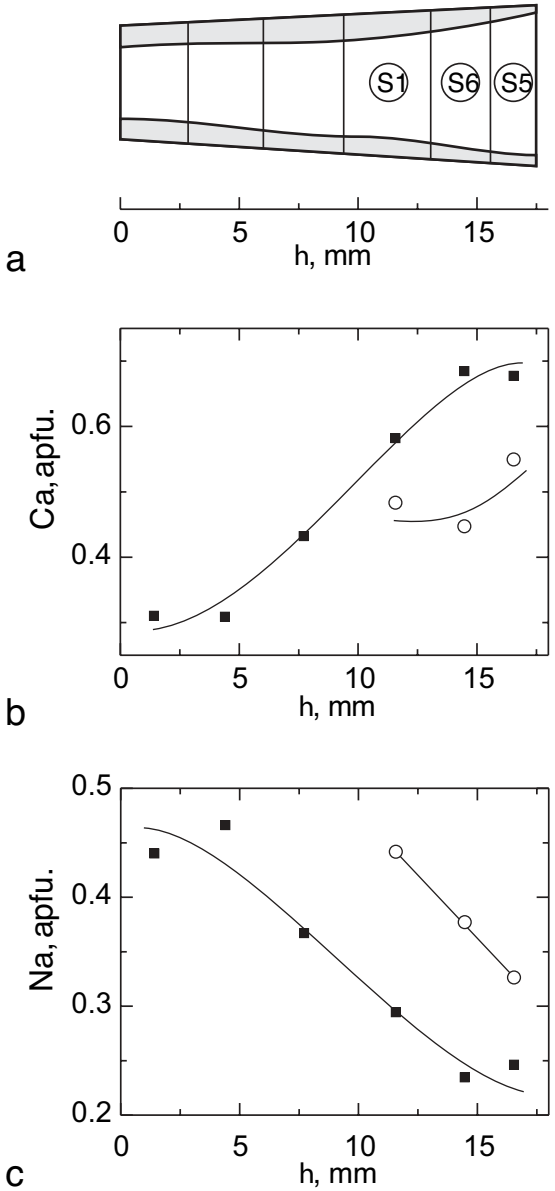

Figure 1. (**a**) Sketch of studied crystal. Gray and white sectors correspond to growth sectors of prisms and pyramids, respectively. The locations of the samples chosen, S1, S6, S5, for X-ray diffraction analysis are indicated. (**b** and **c**) Diagrams illustrating the chemical zoning in Ca and Na along the growth direction [0001] in the growth sectors of {02$\bar{2}$1} (filled squares) and in growth sectors of prisms (circles). Lines are guides to the eye.

Results

Anatomy, chemical composition, and optical anomalies

According to the EPMA (Fig. 1, Table 2) the studied specimen is a solid solution of elbaite $Na(Li_{1.5}Al_{1.5})Al_6(Si_6O_{18})(BO_3)_3(OH)_3(OH,F)$ and liddicoatite $Ca(Li_2Al)Al_6(Si_6O_{18})(BO_3)_3(OH)_3(OH,F)$ with minor rossmanite $(\square)(LiAl_2)Al_6(Si_6O_{18})(BO_3)_3(OH)_3(OH)$ (Hawthorne and Henry 1999). It is important to note a wide variation of the chemical composition within the crystal: the innermost growth zones are predominantly elbaite, whereas the outmost are predominantly liddicoatite (Fig. 1). Compared to the {02$\bar{2}$1} growth sectors, the growth sectors of the prisms are slightly enriched in the elbaite component (Fig. 1), as was also reported by Akizuki et al. (2001).

A typical (0001) cross section of the investigated tourmaline is shown in Figure 2. The crystal is optically biaxial, and the biaxiality is inhomogeneously distributed. The large growth sectors {02$\bar{2}$1} display the highest values of the axial angle $2V$, whereas the growth sectors of the pyramid {10$\bar{1}$1} and of the prism faces {10$\bar{1}$0} and {11$\bar{2}$0} are characterized by lower values of $2V$ (Figs. 2 and 3). Within a given growth sector the planes of the optical axes exhibit similar orientations, varying within a range of 10°. In comparison to the data reported by Akizuki et al. (2001), the

Table 1. Samples and X-ray diffraction experiments

Sample	S1	S6	S5
Position in a crystal (h, mm—see Fig. 1)	11.6	14.5	16.5
Axial angle $2V$, °	11(1)	16(1)	23(1)
Radius r, mm	0.16	0.16	0.125
Diffractometer	APEX II	APEX II	Nicolet-P3/R3
μ, mm^{-1}	1.05	1.06	1.12
h_{min}:h_{max}	–24:25	–22:24	–25:21
k_{min}:k_{max}	–24:25	–23:23	–25:15
l_{min}:l_{max}	–11:10	–10:10	–11:11
$2\Theta_{max}$, °	70.74	65.75	70.06
No. reflections, meas.	77117	56187	16511
Lattice constants:			
Trigonal setting (space group $R3m$)			
a_{trig}, Å	15.845	15.840	15.833
c_{trig}, Å	7.110	7.109	7.103
Triclinic (pseudotrigonal) setting (space groups $R1$ and $P1$)			
a_{trcl}, Å	15.854(3)	15.853(3)	15.845(4)
b_{trcl}, Å	15.843(3)	15.834(3)	15.822(4)
c_{trcl}, Å	7.108(1)	7.109(1)	7.103(2)
α, °	89.944(14)	89.989(14)	89.97(3)
β, °	90.045(15)	90.043(14)	90.07(3)
γ, °	119.975(12)	119.949(12)	119.92(2)
Monoclinic setting* (space group Cm)			
a_{mcl}, Å	27.467(10)	27.472(10)	27.466(16)
b_{mcl}, Å	15.843(3)	15.834(3)	15.822(4)
c_{mcl}, Å	7.108(1)	7.109(1)	7.103(2)
β, °	90.045(15)	90.043(14)	90.07(3)

* Relationship between settings: $a_{mcl} = 2a_{trcl} + b_{trcl}$, $b_{mcl} = b_{trcl}$, $c_{mcl} = c_{trcl}$ (Fig. 5).

Table 2. Chemical composition of samples studied with X-ray diffraction methods, growth sector {02$\bar{2}$1}

Sample	S1	S6	S5
Wt%			
Na_2O	0.99	0.79	0.82
CaO	3.54	4.17	4.08
SiO_2	39.1	39.15	38.72
Al_2O_3	41.94	41.71	42.02
MnO	0.85	1.46	1.68
FeO	0.18	0.12	0.09
TiO_2	0.06	0.06	0.07
F	1.61	1.57	1.22
Formula units			
Na	0.29	0.23	0.25
Ca	0.58	0.68	0.68
ΣX	0.87	0.91	0.93
Al	1.58	1.53	1.67
Li	1.28	1.25	1.09
Mn	0.11	0.19	0.22
Fe	0.02	0.02	0.01
Ti	0.01	0.01	0.01
ΣY	3.00	3.00	3.00
ΣZ = Al	6.00	6.00	6.00
Si	6.00	6.00	6.00
O^{2-}	0.77	0.85	1.21
F	0.78	0.76	0.60
OH	2.45	2.39	2.19

correlation between the optic axial plane orientation and the growth front direction is less clear in our case; nonetheless such a relationship is definitely present. The axial angle increases markedly from the innermost to the outermost growth zones (Fig. 3), suggesting a lowering of the symmetry.

Diffraction pattern

As Wildner and Andrut (2001) and Shtukenberg et al. (2005, 2006) have shown for ugrandite garnets, the acquisition of reliable data on the symmetry of crystals with optical anomalies requires the analysis of the diffraction pattern as well as refinements of the crystal structure in a series of space groups (ideal high-symmetry space group and all possible subgroups). In this study, we also analyzed the crystal symmetry following this procedure.

Although the unit-cell dimensions of the samples studied are approximately trigonal there are significant differences between the lattice constants a and b (up to 6 e.s.d.) as well as less pronounced deviations of the angles α, β, and γ from 90° and 120°, respectively (up to 4 e.s.d., Table 1). These findings suggest lowering of symmetry to triclinic or at least monoclinic. The lattice distortions are close to those reported by Akizuki et al. (2001) for a fragment of the biaxial {02$\bar{2}$1} growth sector ($2V$ = 30°), where the deviations of the unit-cell angles from the ideal values were even more pronounced [a = 15.863(2) Å, b = 15.851(2) Å, c = 7.107(1) Å, α = 90.12(1)°, β = 89.88(1)°, γ = 120.22(1)°].

The next test concerns the intensities of reflections, which are equivalent with respect to the individual symmetry operations in the trigonal space group $R3m$. Such reflections were grouped, and each group was analyzed separately. If the difference of the intensities ($F^2_{max} - F^2_{min}$) within a group exceeded a

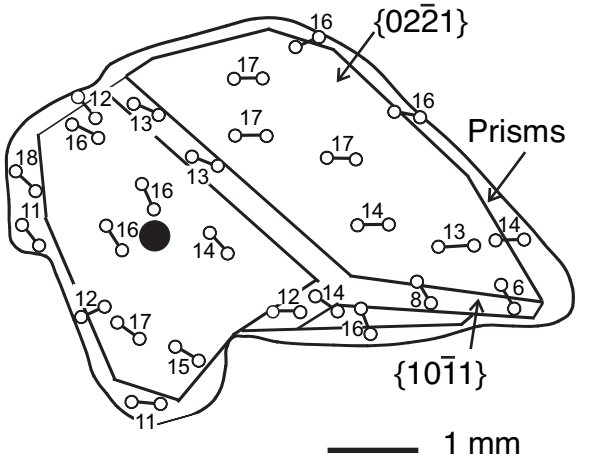

Figure 2. (0001) section at h = 14.5 mm of the tourmaline crystal. The dumb-bells indicate the orientations of the optic axial planes; numbers are $2V$ values in degrees. The filled black circle gives the location of sample S6.

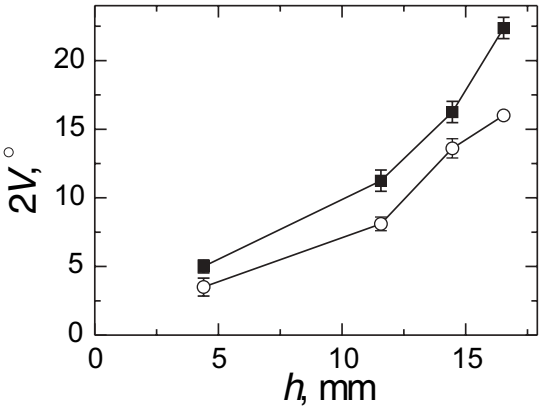

Figure 3. Variation of the axial angle $2V$ along the growth direction [0001] in growth sectors of {02$\bar{2}$1} (filled squares) and of prisms (circles). Lines are guides to the eye.

certain threshold value, the group was considered to violate the symmetry operation. We selected as threshold criteria both the maximum value of the standard deviation (e.s.d.) of the reflection intensities and the largest intensity difference of a Friedel pair of reflections found within a given group of reflections. The results were similar for both criteria, e.g., $F^2_{max} - F^2_{min} > 4|F^2_{hkl} - F^2_{\overline{hkl}}|$ (Fig. 4). The percentages of groups of reflections (P) breaking the symmetry operations are nearly the same except for the mirror plane m_y (Fig. 5a). In this case, only a very small number of groups shows violations, so that m_y can be considered to be present in the crystal structure. Thus, the symmetry of the samples has been lowered, i.e., the crystals are monoclinic or possibly triclinic.

The analysis of the reflection conditions for the samples S1, S6, and S5 revealed 74, 34, and 52 weak reflections with $F^2_o > 4\sigma(F^2_o)$, respectively, which would be forbidden in space group $R3m$. However, closer inspection of these reflections by means of ψ scans carried out for sample S5 left only 3–5 reflections. The

Table 3. Refinements of the tourmaline crystal structure in different space groups

Sample	S1	S6	S5
Space group *R*3*m*			
no. unique reflections	1579	1307	1654
no. reflections > 4σ(F_o)	1570	1301	1644
no. l.s. parameters	91	91	91
R_{int}	0.0504	0.0509	0.0724
R [F_o > 4σ(F_o)]	0.0220	0.0205	0.0270
Rw	0.0872	0.0785	0.0686
Goodness of fit	1.119	1.070	1.211
Extinction coefficient	0.010480	0.010736	0.000983
Weights, k_1, k_2*	0.0640	0.0571	0.0272
	2.7360	3.9506	0.5702
Flack parameter	–0.14(8)	0.06(9)	–0.14(9)
Deepest hole and largest peak	1.11	1.00	1.25
	–0.84	–0.56	–0.93
Space group *Cm*	(mirror plane m_y)		
no. unique reflections	11922	10258	13470
no. reflections > 4σ(F_o)	4004	3404	5293
no. l.s. of parameters	723	723	638
R_{int}	0.0232	0.0255	0.0186
R [F_o > 4σ(F_o)]	0.0211	0.0193	0.0388
Rw	0.0760	0.0905	0.1032
Goodness of fit	1.038	0.946	1.088
Extinction coefficient	0.002886	0.002831	0.000237
Weights, k_1, k_2*	0.0260	0.0400	0.0260
	8.0217	11.0217	18.0217
Flack parameter	–0.08(3)	–0.06(4)	–0.13(5)
Deepest hole and largest peak	1.42	1.12	2.51
	–0.97	–1.28	–1.81
Space group *P*1			
no. unique reflections	22000	18760	16505
no. reflections > 4σ(F_o)	7337	6206	6525
no. l.s. of parameters	1365	1365	1320
R [F_o > 4σ(F_o)]	0.0211	0.0186	0.0315
Rw	0.0777	0.0749	0.0903
Goodness of fit	1.139	1.093	1.300
Extinction coefficient	0.003301	0.003186	0.000260
Weights, k_1, k_2*	0.0200	0.0200	0.0066
	8.0000	8.0000	8.0217
Flack parameter	–0.09(2)	–0.05(3)	–0.03(3)
Deepest hole and largest peak	0.89	0.83	1.20
	–0.84	–0.59	–1.06
Space group *R*1†			
no. unique reflections	7246	6161	5653
no. reflections > 4σ(F_o)	7230	6152	5615
no. l.s. of parameters	452	452	452
R [F_o > 4σ(F_o)]	0.0214	0.0197	0.0281
Rw	0.0629	0.0621	0.0748
Goodness of fit	1.126	1.131	1.067
Extinction coefficient	0.010093	0.011401	0.001147
Weights, k_1, k_2*	0.0240	0.0280	0.0452
	6.3787	5.5295	5.9190
Flack parameter	–0.09(4)	–0.04(4)	–0.08(5)
Deepest hole and largest peak	1.66	1.44	3.21
	–1.28	–1.16	–2.18

* Weighting scheme: weight = $1/\{[\sigma(F_o^2)]^2 + (k_1P)^2 + k_2P\}$, where $P = [\max(F_o^2,0) + 2F_c^2]/3$.
† The space group *R*1 was constructed using pseudohexagonal triclinic cell and adding (1/3, 2/3, 2/3) and (2/3, 1/3, 1/3) translational equivalents to each of the atoms in the asymmetric unit.

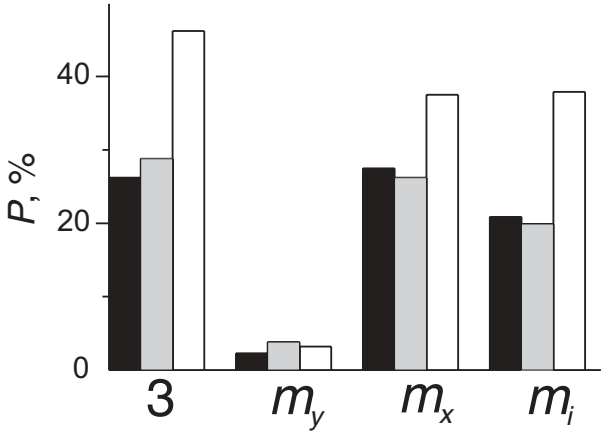

Figure 4. Percentage of groups of reflections (*P*) breaking the indicated symmetry operations, threefold axis, and mirror planes (Fig. 5a). Black, gray, and white bars correspond to samples S1, S6, and S5, respectively.

main part of observed forbidden reflections seems to originate from the multiple scattering phenomenon as well as from the λ/2 contribution, which is strong for the data obtained with the Bruker diffractometer.

In summary, the analysis of the diffraction patterns showed lowering of symmetry either to the monoclinic space group *Cm* ($a_{mcl} = 2a_{tricl} + b_{tricl}$, $b_{mcl} = b_{tricl}$, $c_{mcl} = c_{tricl}$; see Fig. 5a) or to the pseudotrigonal triclinic space groups *R*1 or *P*1. The space group *R*1 seems to be more appropriate choice among triclinic space groups, since according to analysis of the reflection conditions the *R*-lattice is likely to be present in the non-trigonal tourmaline crystal structures.

Crystal structure refinement

To determine the crystal symmetry and to elucidate the origin of the symmetry reduction the crystal structures of the three samples were refined in space group *R*3*m* as well as in its subgroups: monoclinic *Cm* (with orientation corresponding to the mirror plane m_y, for which the least number of violations of reflection equivalence were observed; see Fig. 4), and triclinic *R*1 and *P*1 (Table 3). A non-standard space group *R*1 was constructed taking a psuedohexagonal triclinic cell and adding (1/3, 2/3, 2/3) and (2/3, 1/3, 1/3) translational equivalents to each of the atoms in their asymmetric unit, as though it were actually a rhombohedral lattice in a hexagonal setting. That is, *R*1 means that even though this is a triclinic cell, each atom has translational equivalents at (*x*+1/3, *y*+2/3, *z*+2/3) and (*x*+2/3, *y*+1/3, *z*+1/3). Introduction of this space group turns out to be very useful for description of the dissymmetrized tourmaline crystal structures and its comparison with the ideal trigonal crystal structure. The cation distributions found in the course of the refinements in *R*1 and *P*1 were consistent with the ordering scheme revealed for space group *Cm*.

Since the atomic arrangements in the low-symmetry space groups are almost the same as in *R*3*m*, their refinements become less stable. Therefore, we failed to refine positional and displacement parameters of the hydrogen atoms and they were omitted. Also we could not refine reliably fractions of F and OH at OW1 sites and only site occupancies by F are given. We neglected small admixture of Mn (up to 0.08 apfu, Table 2) and assumed the Y sites to be fully occupied by Al and Li. The final values of the atomic coordinates, displacement parameters, and site occupancies are listed in Table 4 for the initial space group *R*3*m* along with those obtained for the space groups *Cm* and *R*1 (Tables 5–6). We do not present data on the space group *P*1, since the crystal structure distortions found for this space group are reproduced for the more symmetrical space group *R*1 (see below).

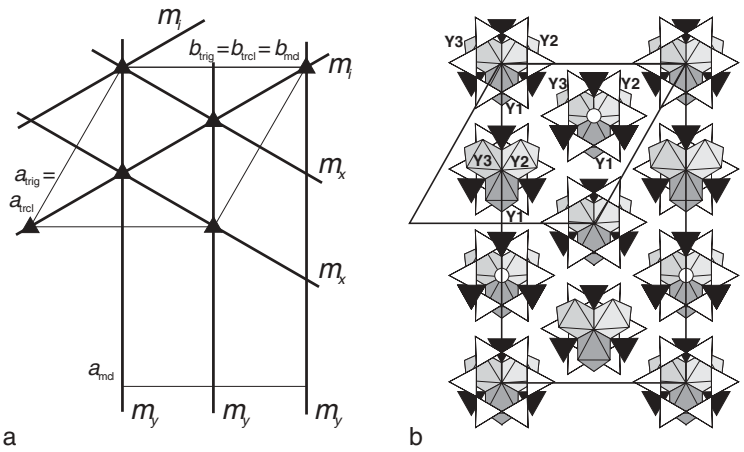

FIGURE 5. (**a**) Relationship between trigonal (space group $R3m$), pseudotrigonal (triclinic, space groups $P1$ and $R1$), and monoclinic (space group Cm) cells. (**b**) Schematic projection of the tourmaline structure on the (0001) plane. The different Al,Li occupancies of the Y octahedra corresponding to refinements in the space group $R1$ are indicated by different gray scales. The white and black triangles represent SiO_4 tetrahedra and BO_3 groups, respectively.

TABLE 4. Occupancies, fractional atomic coordinates and equivalent isotropic displacement parameters for the samples S1 (upper line), S6 (middle line) and S5 (lower line) with e.s.d.s in parentheses in space group $R3m$

Site	Composition/ Site occupancy	x	y	z	U_{eq}, Å^2
X	$Na_{0.21(2)}Ca_{0.79(2)}$	0	0	0.23764(18)	0.0165(4)
	$Na_{0.19(2)}Ca_{0.81(2)}$	0	0	0.2381(2)	0.0186(5)
	$Na_{0.47(2)}Ca_{0.53(2)}$	0	0	0.23855(17)	0.0108(4)
Y	$Al_{0.498(9)}Li_{0.502(9)}$	0.12400(11)	$x/2$	0.6343(2)	0.0084(5)
	$Al_{0.485(9)}Li_{0.515(9)}$	0.12413(12)	$x/2$	0.6339(2)	0.0079(5)
	$Al_{0.449(7)}Li_{0.551(7)}$	0.12432(11)	$x/2$	0.6349(2)	0.0068(4)
Z	$Al_{1.0}$	0.29679(4)	0.25969(4)	0.61176(10)	0.00512(14)
	$Al_{1.0}$	0.29675(4)	0.25965(4)	0.61145(12)	0.00528(16)
	$Al_{1.0}$	0.29680(4)	0.25967(4)	0.61180(9)	0.00578(11)
B	1	0.10906(9)	$2x$	0.4548(4)	0.0054(4)
	1	0.10898(11)	$2x$	0.4544(4)	0.0055(4)
	1	0.10909(10)	$2x$	0.4553(3)	0.0062(3)
T	$Si_{0.97(1)}B_{0.03(1)}$	0.19212(3)	0.19013(3)	0	0.00356(16)
	$Si_{0.96(1)}B_{0.04(1)}$	0.19210(3)	0.19012(4)	0	0.00332(19)
	$Si_{0.95(1)}B_{0.05(1)}$	0.19208(3)	0.19004(3)	0	0.00393(13)
O1W	$F_{0.98(2)}$	0	0	0.7892(7)	0.052(2)
	$F_{0.93(2)}$	0	0	0.7877(7)	0.049(2)
	$F_{0.99(2)}$	0	0	0.7878(6)	0.055(2)
O2	1	0.05982(8)	$2x$	0.4810(3)	0.0167(4)
	1	0.05972(8)	$2x$	0.4801(4)	0.0159(5)
	1	0.05959(7)	$2x$	0.4804(3)	0.0163(4)
O3	1	0.26907(16)	$x/2$	0.5094(3)	0.0096(3)
	1	0.26893(18)	$x/2$	0.5101(3)	0.0099(4)
	1	0.26944(16)	$x/2$	0.5100(3)	0.0101(3)
O4	1	0.09223(7)	$2x$	0.0748(3)	0.0074(3)
	1	0.09230(8)	$2x$	0.0750(3)	0.0080(4)
	1	0.09223(7)	$2x$	0.0748(2)	0.0079(3)
O5	1	0.18395(14)	$x/2$	0.0966(2)	0.0078(3)
	1	0.18399(16)	$x/2$	0.0964(3)	0.0083(4)
	1	0.18372(14)	$x/2$	0.0959(2)	0.0086(3)
O6	1	0.19606(9)	0.18617(10)	0.7758(2)	0.0067(2)
	1	0.19596(10)	0.18618(11)	0.7758(2)	0.0072(3)
	1	0.19603(9)	0.18608(9)	0.77598(16)	0.0073(2)
O7	1	0.28600(9)	0.28539(9)	0.08139(17)	0.0059(2)
	1	0.28594(10)	0.28535(10)	0.08155(19)	0.0059(3)
	1	0.28604(9)	0.28522(8)	0.08147(15)	0.0067(2)
O8	1	0.20937(9)	0.26982(10)	0.44136(19)	0.0068(2)
	1	0.20955(11)	0.26990(10)	0.4413(2)	0.0067(3)
	1	0.20951(9)	0.27013(9)	0.44175(18)	0.00751(19)

Crystal structure distortions

The main unit of the tourmaline crystal structure is an antigorite fragment $XY_3T_6O_{18}$ (Belov 1976) consisting of three layers parallel to (0001). As viewed in Figure 5b, the lowermost layer is composed of three edge sharing Y-octahedra in a closest-packed arrangement. In the analyzed crystals, the Y sites are occupied by Al, Li, and minor amounts of Fe, Mn, and Ti. A ring of six SiO_4 tetrahedra is located above the Y-octahedra. The uppermost layer contains the nine coordinated X site variably occupied by the large cations Na and Ca. The trigonal unit cell of tourmaline contains three such antigorite fragments that are related by R-translation symmetry and therefore located at different heights (Fig. 5b). Each antigorite fragment is cross-linked to other fragments by six Z octahedra sharing edges with the Y octahedra.

This general topology of the crystal structure is preserved in the biaxial elbaite-liddicoatite tourmalines, where the symmetry reduction mainly results from partial cation ordering at the octahedral Y sites. In the monoclinic space group Cm, the Y site splits into six independent sites (Table 5). However, occupancies of these six sites can be grouped into two groups with significantly different occupancies $x_{Al} = Al/(Al + Li)$ (differences in occupancies equal 0.14, 0.14, and 0.29 for the samples S1, S6, and S5, respectively), whereas differences within these groups are small (for the samples S1 and S6 less than 0.004 or 2 e.s.d., for the sample S5, however, up to 0.034 or 17 e.s.d.). In the trigonal setting, the sites, which belong to the same group, are related to each other by means of R translations. Thus, the R symmetry appears still present in the crystal structure in conformity with the analysis of the diffraction pattern. More significant violations of R translations found for the sample S5 seem to be a result of an imperfect crystal structure refinement process in this case, and these violations were not confirmed by the subsequent refinement in the less symmetrical triclinic space group $P1$.

For space group $P1$ nine non-equivalent Y sites must be considered. In this case, however, the occupancies of the sites related by R symmetry varied at most by 0.016. This difference corresponds to 3 e.s.d.s, which also confirms the presence of R translations. This conclusion is further supported by Y-O cation-oxygen bond lengths, for which in space group $P1$, the maximum difference between Y octahedra related by R translation does not exceed 0.005 Å (i.e., less than 1 e.s.d.) for all three samples. Thus, we describe the tourmaline crystal structures in space group $R1$,

for which preservation of *R* translation significantly reduces the number of independent atomic sites.

In the triclinic space group *R*1, the Y site splits into three independent sites, so that the three Y sites in one and the same antigorite fragment can acquire different occupancies (Fig. 5b). The observed occupancies of these Y sites correlate well with the mean octahedral cation-oxygen distances <Y-O> (Tables 6–7, Fig. 6).

As can be seen from Tables 5–6 and Figure 6, the Y1 site contains significantly more Al than the two other sites, Y2 and Y3, respectively, whose Al occupancies are very close to one another. The difference between the former and the mean of the latter two occupancies increases with the value of the axial angle 2*V*, attaining 0.32 for sample S5 (Fig. 7). Thus, neglecting the small differences in the occupancies of the Y2 and Y3 sites, the

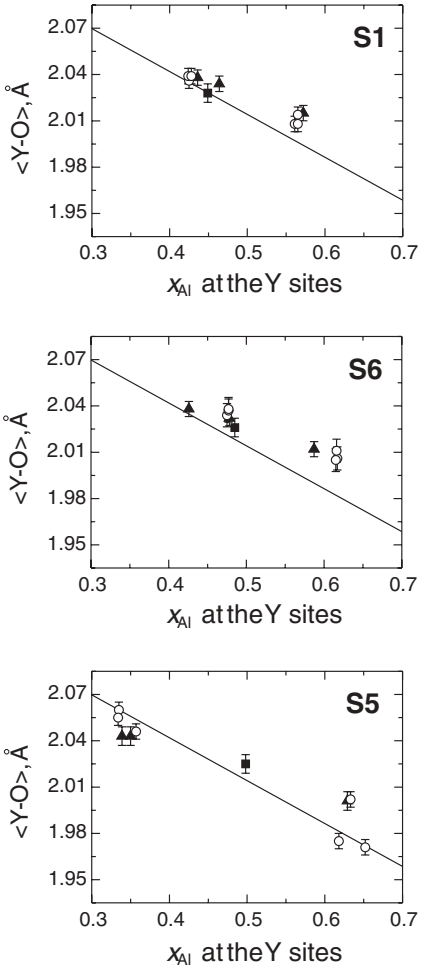

FIGURE 6. Mean cation-oxygen bond lengths <Y-O> vs. x_{Al}, the proportion of Al on the Y sites in the samples S1, S6, and S5. Squares = refinements in space group *R*3*m*, circles = in *Cm*, and triangles = in *R*1. The solid lines present corresponding mean data from four samples of the elbaite-liddicoatite solid solution with minor (in sum less than 0.08 apfu) impurities of Mn, Mg, Fe, and other elements occupying the Y sites (Nuber and Schmetzer 1981; Burns et al. 1994; MacDonald and Hawthorne 1995).

TABLE 5. Occupancies, fractional atomic coordinates, and equivalent displacement parameters for the samples S1 (upper line), S6 (middle line) and S5 (lower line) with e.s.d. values in parentheses in space group *Cm*

Site	Composition/ Site occupancy	*x*	*y*	*z*	U_{eq}, Å^2
X1	$Na_{0.41(1)}Ca_{0.59(1)}$	0	0	0.23813(12)	0.0136(2)
	$Na_{0.33(1)}Ca_{0.67(1)}$	0	0	0.23827(12)	0.0153(2)
	$Na_{0.42(1)}Ca_{0.58(1)}$	0	0	0.23951(7)	0.01419(10)
X2	$Na_{0.39(1)}Ca_{0.61(1)}$	0.16655(3)	0.5	0.90485(12)	0.0124(2)
	$Na_{0.33(1)}Ca_{0.67(1)}$	0.16658(3)	0.5	0.90497(12)	0.0151(2)
	$Na_{0.50(1)}Ca_{0.50(1)}$	0.16620(2)	0.5	0.90592(6)	0.00975(10)
X3	$Na_{0.40(1)}Ca_{0.60(1)}$	0.83322(3)	0.5	0.57159(12)	0.0134(2)
	$Na_{0.33(1)}Ca_{0.67(1)}$	0.83328(3)	0.5	0.57165(13)	0.0154(2)
	$Na_{0.53(1)}Ca_{0.47(1)}$	0.83313(2)	0.5	0.57283(6)	0.00724(9)
Y11	$Al_{0.565(4)}Li_{0.435(4)}$	0.06246(5)	0	0.6351(2)	0.0067(3)
	$Al_{0.616(4)}Li_{0.384(4)}$	0.06260(5)	0	0.6351(2)	0.0089(4)
	$Al_{0.633(2)}Li_{0.367(2)}$	0.06284(3)	0	0.63566(10)	0.00484(14)
Y12	$Al_{0.565(4)}Li_{0.435(4)}$	0.22914(5)	0.5	0.3015(2)	0.0058(4)
	$Al_{0.615(4)}Li_{0.385(4)}$	0.22924(5)	0.5	0.3017(2)	0.0082(4)
	$Al_{0.618(2)}Li_{0.382(2)}$	0.22974(3)	0.5	0.30348(11)	0.00574(15)
Y13	$Al_{0.561(4)}Li_{0.439(4)}$	0.89589(5)	0.5	0.9682(2)	0.0083(4)
	$Al_{0.617(4)}Li_{0.383(4)}$	0.89594(5)	0.5	0.9684(2)	0.0088(4)
	$Al_{0.652(2)}Li_{0.348(2)}$	0.89667(3)	0.5	0.96943(10)	0.00757(16)
Y21	$Al_{0.425(2)}Li_{0.575(2)}$	−0.03086(4)	0.09290(8)	0.63471(18)	0.0085(3)
	$Al_{0.475(3)}Li_{0.525(3)}$	−0.03068(4)	0.09274(9)	0.63469(19)	0.0119(3)
	$Al_{0.357(2)}Li_{0.643(2)}$	−0.03073(3)	0.09246(6)	0.63539(13)	0.01126(18)
Y22	$Al_{0.428(3)}Li_{0.572(3)}$	0.13583(4)	0.59283(9)	0.30126(19)	0.0080(3)
	$Al_{0.477(3)}Li_{0.523(3)}$	0.13601(4)	0.59280(9)	0.30136(18)	0.0118(4)
	$Al_{0.335(2)}Li_{0.665(2)}$	0.13622(3)	0.59273(5)	0.30388(11)	0.00471(15)
Y23	$Al_{0.424(3)}Li_{0.576(3)}$	0.80248(4)	0.40707(9)	0.96795(19)	0.0087(3)
	$Al_{0.477(3)}Li_{0.523(3)}$	0.80265(4)	0.40720(9)	0.96804(19)	0.0114(4)
	$Al_{0.334(2)}Li_{0.666(2)}$	0.80283(3)	0.40686(5)	0.96672(12)	0.00651(17)
Z1	$Al_{1.0}$	−0.01828(2)	0.27766(4)	0.61194(9)	0.00572(13)
	$Al_{1.0}$	−0.01814(2)	0.27757(5)	0.61192(9)	0.00534(15)
	$Al_{1.0}$	−0.017996(13)	0.27699(2)	0.61290(5)	0.00578(7)
Z2	$Al_{1.0}$	0.14891(2)	0.88816(4)	0.61228(9)	0.00571(13)
	$Al_{1.0}$	0.14905(2)	0.88815(5)	0.61241(9)	0.00521(15)
	$Al_{1.0}$	0.149577(13)	0.88750(2)	0.61349(5)	0.00501(7)
Z3	$Al_{1.0}$	0.87053(2)	0.83273(4)	0.61199(9)	0.00563(13)
	$Al_{1.0}$	0.87070(2)	0.83276(5)	0.61202(9)	0.00520(15)
	$Al_{1.0}$	0.871025(13)	0.83240(2)	0.61273(5)	0.00523(7)
Z4	$Al_{1.0}$	0.14840(2)	0.77764(5)	0.27858(9)	0.00567(14)
	$Al_{1.0}$	0.14852(2)	0.77759(5)	0.27860(9)	0.00535(15)
	$Al_{1.0}$	0.148931(13)	0.77713(2)	0.27908(5)	0.00502(7)
Z5	$Al_{1.0}$	0.31558(2)	0.38815(4)	0.27891(9)	0.00574(14)
	$Al_{1.0}$	0.31571(2)	0.38816(5)	0.27906(9)	0.00535(15)
	$Al_{1.0}$	0.316111(13)	0.38761(2)	0.27974(5)	0.00623(7)
Z6	$Al_{1.0}$	0.03720(2)	0.33274(4)	0.27861(9)	0.00564(14)
	$Al_{1.0}$	0.03737(2)	0.33273(5)	0.27867(9)	0.00532(15)
	$Al_{1.0}$	0.037741(13)	0.33262(2)	0.28000(5)	0.00489(7)
Z7	$Al_{1.0}$	0.81505(2)	0.77765(5)	0.94524(9)	0.00577(14)
	$Al_{1.0}$	0.81519(2)	0.77757(5)	0.94528(9)	0.00541(16)
	$Al_{1.0}$	0.815349(13)	0.77709(2)	0.94579 (5)	0.00589(7)
Z8	$Al_{1.0}$	−0.01776(2)	0.38820(5)	0.94561(9)	0.00577(15)
	$Al_{1.0}$	−0.01762(2)	0.38813(5)	0.94575(9)	0.00534(16)
	$Al_{1.0}$	−0.017213(13)	0.38772(2)	0.94692(5)	0.00504(7)
Z9	$Al_{1.0}$	0.70387(2)	0.33274(5)	0.94527(9)	0.00568(15)
	$Al_{1.0}$	0.70404(2)	0.33275(5)	0.94531(9)	0.00528(16)
	$Al_{1.0}$	0.704299(14)	0.33260(2)	0.94584(5)	0.00616(7)

TABLE 5. —*CONTINUED*

Site	Composition/ Site occupancy	*x*	*y*	*z*	U_{eq}, Å^2
B1	1	0.05504(8)	0.16340(14)	0.4556(3)	0.0059(4)
	1	0.05515(8)	0.16336(17)	0.4551(3)	0.0059(5)
	1	0.05610(4)	0.16379(8)	0.45790(17)	0.00522(17)
B2	1	0.89133(10)	0	0.4547(4)	0.0064(6)
	1	0.89151(12)	0	0.4546(5)	0.0060(7)
	1	0.89156(6)	0	0.4560(2)	0.0060(3)
B3	1	0.22172(8)	0.66339(16)	0.1222(3)	0.0061(5)
	1	0.22182(8)	0.66329(17)	0.1219(3)	0.0054(6)
	1	0.22222(4)	0.66318(8)	0.12222(18)	0.00653(18)
B4	1	0.05795(11)	0.5	0.1213(5)	0.0062(7)
	1	0.05816(12)	0.5	0.1208(5)	0.0050(8)
	1	0.05931(6)	0.5	0.1204(3)	0.0067(3)
B5	1	0.88835(8)	0.33657(17)	0.7889(3)	0.0057(5)
	1	0.88854(8)	0.33658(18)	0.7886(3)	0.0059(6)
	1	0.88896(4)	0.33741(8)	0.78994(18)	0.00593(18)
B6	1	0.72461(11)	0.5	0.7875(5)	0.0051(7)
	1	0.72480(12)	0.5	0.7877(5)	0.0050(8)
	1	0.72411(6)	0.5	0.7897(2)	0.0047(2)
T1	$Si_{0.98(1)}B_{0.02(1)}$	−0.00071(2)	0.19087(3)	0	0.00456(12)
	$Si_{0.99(1)}B_{0.01(1)}$	−0.00059(2)	0.19083(4)	0	0.00426(14)
	$Si_{0.99(1)}B_{0.01(1)}$	−0.000322(12)	0.190633(19)	0	0.00520(6)
T2	$Si_{0.99(1)}B_{0.01(1)}$	0.096359(19)	0.90585(4)	0.00090(8)	0.00441(13)
	$Si_{0.99(3)}B_{0.01(1)}$	0.09653(2)	0.90586(4)	0.00101(8)	0.00418(15)
	$Si_{1.00(1)}$	0.096886(11)	0.906056(19)	0.00266(4)	0.00466(6)
T3	$Si_{0.99(1)}B_{0.01(1)}$	0.905096(19)	0.90293(4)	−0.00011(8)	0.00451(13)
	$Si_{1.01(1)}$	0.90522(2)	0.90289(4)	−0.00002(8)	0.00419(15)
	$Si_{0.99(1)}B_{0.01(1)}$	0.905317(11)	0.90287(2)	0.00058(4)	0.00399(6)
T4	$Si_{0.98(1)}B_{0.02(1)}$	0.16596(2)	0.69087(4)	0.66668(8)	0.00455(13)
	$Si_{0.99(1)}B_{0.02(1)}$	0.16608(2)	0.69085(4)	0.66676(9)	0.00424(15)
	$Si_{0.99(1)}B_{0.01(1)}$	0.166377(12)	0.690740(19)	0.66713(5)	0.00433(6)
T5	$Si_{0.99(1)}B_{0.01(1)}$	0.26302(2)	0.40585(4)	0.66758(8)	0.00445(14)
	$Si_{0.99(1)}B_{0.01(1)}$	0.26317(2)	0.40587(4)	0.66768(8)	0.00405(16)
	$Si_{1.00(1)}$	0.263468(11)	0.40573(2)	0.66871(4)	0.00459(6)
T6	$Si_{0.99(1)}B_{0.01(1)}$	0.07177(2)	0.40290(4)	0.66657(8)	0.00440(14)
	$Si_{1.00(1)}$	0.07190(2)	0.40289(4)	0.66660(8)	0.00457(15)
	$Si_{1.00(1)}$	0.071962(12)	0.402759(19)	0.66684(4)	0.00450(6)
T7	$Si_{0.98(1)}B_{0.02(1)}$	0.83262(2)	0.69086(4)	0.33331(9)	0.00438(14)
	$Si_{0.99(1)}B_{0.01(1)}$	0.83277(2)	0.69082(4)	0.33334(9)	0.00460(16)
	$Si_{0.99(1)}B_{0.01(1)}$	0.833103(12)	0.690434(18)	0.33423(5)	0.00424(6)
T8	$Si_{0.99(1)}B_{0.01(1)}$	0.92971(2)	0.40585(4)	0.33425(8)	0.00442(14)
	$Si_{0.99(1)}B_{0.01(1)}$	0.92984(2)	0.40585(4)	0.33435(9)	0.00394(16)
	$Si_{1.00(1)}$	0.930136(12)	0.40578(2)	0.33543(4)	0.00421(6)
T9	$Si_{0.99(1)}B_{0.01(1)}$	0.73845(2)	0.40290(4)	0.33323(8)	0.00452(14)
	$Si_{1.01(1)}$	0.73858(2)	0.40288(4)	0.33330(9)	0.00466(16)
	$Si_{0.99(1)}B_{0.01(1)}$	0.739077(12)	0.40291(2)	0.33367(5)	0.00491(6)
O11W	$F_{1.03(1)}$	0	0	0.7891(3)	0.0537(13)
	$F_{1.22(1)}$	0	0	0.7888(3)	0.0579(14)
	$F_{0.97(1)}$	0	0	0.7899(3)	0.0499(5)
O12W	$F_{1.03(1)}$	0.16822(15)	0.5	0.4554(4)	0.0524(11)
	$F_{1.19(1)}$	0.16823(15)	0.5	0.4578(4)	0.0673(10)
	$F_{1.01(1)}$	0.17384(6)	0.5	0.4560(3)	0.0347(4)
O13W	$F_{1.03(1)}$	0.83500(15)	0.5	0.1222(4)	0.0531(11)
	$F_{1.19(1)}$	0.83495(14)	0.5	0.1223(4)	0.0670(12)
	$F_{0.98(1)}$	0.84030(7)	0.5	0.1227(3)	0.0363(4)
O21	1	0.03129(6)	0.08863(11)	0.4816(2)	0.0170(4)
	1	0.03147(6)	0.08845(12)	0.4822(2)	0.0166(4)
	1	0.03274(3)	0.08759(6)	0.48234(13)	0.01178(15)
O22	1	−0.05969(7)	0	0.4790(3)	0.0161(6)
	1	−0.05947(8)	0	0.4794(3)	0.0149(6)
	1	−0.05895(5)	0	0.4774(2)	0.0190(4)
O23	1	0.19793(6)	0.58864(12)	0.1484(2)	0.0166(4)
	1	0.19814(6)	0.58852(12)	0.1489(2)	0.0167(5)
	1	0.19971(4)	0.58713(7)	0.14851(15)	0.0206(2)
O24	1	0.10694(8)	0.5	0.1454(3)	0.0157(6)
	1	0.10721(8)	0.5	0.1462(3)	0.0155(6)
	1	0.10702(5)	0.5	0.14566(18)	0.0138(3)
O25	1	0.86460(6)	0.58870(12)	0.8150(2)	0.0171(4)
	1	0.86472(6)	0.58849(12)	0.8155(2)	0.0163(5)
	1	0.86607(3)	0.58736(7)	0.81801(14)	0.01359(17)
O26	1	0.77373(7)	0.5	0.8123(3)	0.0166(6)
	1	0.77384(8)	0.5	0.8128(3)	0.0156(7)
	1	0.77389(4)	0.5	0.81083(19)	0.0118(3)
O31	1	0.13399(8)	0	0.5104(3)	0.0107(5)
	1	0.13390(8)	0	0.5112(3)	0.0095(5)
	1	0.13322(5)	0	0.51091(19)	0.0110(3)
O32	1	−0.06727(5)	0.20242(10)	0.5096(2)	0.0101(3)
	1	−0.06710(5)	0.20239(11)	0.5101(2)	0.0103(4)
	1	−0.06737(3)	0.20278(6)	0.50986(12)	0.00988(18)
O33	1	0.30065(8)	0.5	0.1771(3)	0.0103(5)
	1	0.30054(8)	0.5	0.1778(3)	0.0101(6)
	1	0.30070(4)	0.5	0.17849 (17)	0.00790(19)
O34	1	0.09940(5)	0.70244(11)	0.1762(2)	0.0102(4)
	1	0.09957(5)	0.70238(11)	0.1768(2)	0.0102(4)
	1	0.09955(3)	0.70362(6)	0.17775(12)	0.01136(19)
O35	1	−0.03268(8)	0.5	0.8437(3)	0.0102(5)
	1	−0.03271(8)	0.5	0.8445(3)	0.0102(6)
	1	−0.03289(5)	0.5	0.84534(17)	0.0107(3)
O36	1	0.76606(5)	0.29761(11)	0.8428(2)	0.0102(4)
	1	0.76623(5)	0.29767(11)	0.8434(2)	0.0101(4)
	1	0.76629(3)	0.29725(6)	0.84240(12)	0.00845(18)
O41	1	0.04638(5)	0.13818(10)	0.0752(2)	0.0083(3)
	1	0.04647(5)	0.13805(11)	0.0753(2)	0.0079(4)
	1	0.04664(3)	0.13772(7)	0.07674(13)	0.0128(2)
O42	1	−0.09243(7)	0	0.0746(3)	0.0083(4)
	1	−0.09227(8)	0	0.0747(3)	0.0078(5)
	1	−0.09232(4)	0	0.07576(17)	0.0072(2)
O43	1	0.21307(5)	0.63815(11)	0.7417(2)	0.0079(3)
	1	0.21314(5)	0.63808(11)	0.7420(2)	0.0077(4)
	1	0.21364(3)	0.63834(5)	0.74346(12)	0.00645(13)
O44	1	0.07426(7)	0.5	0.7413(3)	0.0080(5)
	1	0.07445(8)	0.5	0.7414(3)	0.0079(5)
	1	0.07397(5)	0.5	0.74201(18)	0.0117(3)
O45	1	0.87973(5)	0.36188(11)	0.4084(2)	0.0080(4)
	1	0.87980(5)	0.36194(11)	0.4086(2)	0.0077(4)
	1	0.87979(3)	0.36307(5)	0.40881(11)	0.00420(12)
O46	1	0.74097(7)	0.5	0.4080(3)	0.0084(5)
	1	0.74107(8)	0.5	0.4081(3)	0.0078(5)
	1	0.74180(4)	0.5	0.40801(16)	0.0049(2)
O51	1	0.09285(8)	0	0.0972(3)	0.0081(5)
	1	0.09290(8)	0	0.0974(3)	0.0082(5)
	1	0.09385(5)	0	0.09842(17)	0.0102(3)
O52	1	−0.04572(5)	0.13772(10)	0.0960(2)	0.0084(3)
	1	−0.04553(5)	0.13768(11)	0.0960(2)	0.0083(4)
	1	−0.04532(3)	0.13736(6)	0.09596(12)	0.00929(17)

TABLE 5. —*CONTINUED*

Site	Composition/ Site occupancy	*x*	*y*	*z*	U_{eq}, Å^2
O53	1	0.25950(7)	0.5	0.7638(3)	0.0086(5)
	1	0.25957(8)	0.5	0.7641(3)	0.0078(5)
	1	0.26006(4)	0.5	0.76602(18)	0.0094(3)
O54	1	0.12095(5)	0.63780(11)	0.7626(2)	0.0084(3)
	1	0.12117(5)	0.63761(11)	0.7627(2)	0.0081(4)
	1	0.12150(3)	0.63764(6)	0.76305(12)	0.00913(18)
O55	1	0.92611(7)	0.5	0.4303(3)	0.0081(5)
	1	0.92623(8)	0.5	0.4307(3)	0.0083(6)
	1	0.92664(4)	0.5	0.43148(17)	0.0067(2)
O56	1	0.78763(5)	0.36231(11)	0.4293(2)	0.0083(4)
	1	0.78780(5)	0.36236(11)	0.4293(2)	0.0080(4)
	1	0.78805(3)	0.36320(5)	0.42983(12)	0.00626(13)
O61	1	–0.00436(4)	0.19103(10)	0.77639(18)	0.0075(3)
	1	–0.00420(4)	0.19080(12)	0.77638(19)	0.0076(4)
	1	–0.00351(3)	0.19146(5)	0.77681(11)	0.00633(16)
O62	1	0.09822(5)	0.91229(10)	0.7764(2)	0.0075(3)
	1	0.09825(5)	0.91243(11)	0.7766(2)	0.0076(4)
	1	0.09871(3)	0.91294(5)	0.77741(12)	0.00705(16)
O63	1	0.90691(5)	0.89698(10)	0.7764(2)	0.0075(3)
	1	0.90713(5)	0.89695(11)	0.7764(2)	0.0072(4)
	1	0.90683(3)	0.89642(5)	0.77646(12)	0.00759(17)
O64	1	0.16236(5)	0.69093(10)	0.4431(2)	0.0076(3)
	1	0.16246(6)	0.69084(10)	0.4431(2)	0.0068(4)
	1	0.16275(3)	0.69063(6)	0.44319(12)	0.00845(14)
O65	1	0.26491(5)	0.41222(11)	0.4431(2)	0.0074(3)
	1	0.26492(5)	0.41243(11)	0.4432(2)	0.0075(4)
	1	0.26524(3)	0.41262(6)	0.44416(12)	0.00900(18)
O66	1	0.07358(5)	0.39701(10)	0.4432(2)	0.0076(3)
	1	0.07381(5)	0.39697(11)	0.4431(2)	0.0075(4)
	1	0.07375(3)	0.39710(6)	0.44389(12)	0.00849(17)
O67	1	0.82901(6)	0.69096(10)	0.1096(2)	0.0073(3)
	1	0.82913(6)	0.69083(10)	0.1099(2)	0.0070(4)
	1	0.82973(3)	0.69029(5)	0.11016(12)	0.00772(14)
O68	1	0.93156(5)	0.41225(11)	0.1098(2)	0.0073(4)
	1	0.93161(5)	0.41238(11)	0.1098(2)	0.0070(4)
	1	0.93177(3)	0.41264(5)	0.11004(11)	0.00576(16)
O69	1	0.74028(5)	0.39691(11)	0.1097(2)	0.0076(4)
	1	0.74048(5)	0.39697(11)	0.1099(2)	0.0073(4)
	1	0.74067(3)	0.39686(6)	0.11080(11)	0.00639(17)
O71	1	–0.00013(5)	0.28551(9)	0.08194(19)	0.0064(3)
	1	0.00001(5)	0.28549(10)	0.0819(2)	0.0058(4)
	1	–0.00008(3)	0.28546(5)	0.08325(11)	0.00587(16)
O72	1	0.14323(5)	0.85718(10)	0.0815(2)	0.0065(3)
	1	0.14341(5)	0.85719(10)	0.0817(2)	0.0062(3)
	1	0.14392(3)	0.85753(5)	0.08121(12)	0.00688(16)
O73	1	0.85762(4)	0.85654(10)	0.0818(2)	0.0065(3)
	1	0.85779(5)	0.85652(11)	0.0818(2)	0.0065(3)
	1	0.85803(3)	0.85659(5)	0.08314(11)	0.00587(16)
O74	1	0.16656(5)	0.78554(10)	0.7486(2)	0.0062(3)
	1	0.16668(5)	0.78558(10)	0.7486(2)	0.0063(4)
	1	0.16698(3)	0.78502(5)	0.75018(12)	0.00739(17)
O75	1	0.30988(5)	0.35714(10)	0.7481(2)	0.0064(3)
	1	0.31008(5)	0.35722(11)	0.7484(2)	0.0062(4)
	1	0.31011(3)	0.35590(6)	0.74858(12)	0.00813(17)
O76	1	0.02428(5)	0.35661(10)	0.7484(2)	0.0064(3)
	1	0.02448(5)	0.35651(10)	0.7485(2)	0.0060(4)
	1	0.02458(3)	0.35646(6)	0.74749(12)	0.00781(17)
O77	1	0.83322(5)	0.78549(10)	0.4153(2)	0.0064(3)
	1	0.83337(5)	0.78549(11)	0.4153(2)	0.0061(4)
	1	0.83357(3)	0.78536(5)	0.41565(11)	0.00533(16)
O78	1	–0.02343(5)	0.35715(10)	0.4149(2)	0.0068(3)
	1	–0.02324(5)	0.35723(11)	0.4149(2)	0.0059(4)
	1	–0.02338(3)	0.35703(5)	0.41628(11)	0.00424(16)
O79	1	0.69095(5)	0.35655(10)	0.4152(2)	0.0064(3)
	1	0.69113(5)	0.35652(11)	0.4152(2)	0.0059(4)
	1	0.69139(3)	0.35645(5)	0.41649(12)	0.00518(16)
O81	1	0.03040(5)	0.23908(10)	0.4414(2)	0.0077(3)
	1	0.03053(5)	0.23891(11)	0.4413(2)	0.0076(4)
	1	0.03063(3)	0.23841(5)	0.44118(12)	0.00741(13)
O82	1	0.10531(5)	0.83437(10)	0.4426(2)	0.0075(3)
	1	0.10545(5)	0.83442(11)	0.4426(2)	0.0070(4)
	1	0.10607(3)	0.83348(5)	0.44439(11)	0.00632(16)
O83	1	0.86516(5)	0.92536(10)	0.4418(2)	0.0072(3)
	1	0.86538(5)	0.92530(11)	0.4417(2)	0.0068(3)
	1	0.86554(3)	0.92528(5)	0.44191(12)	0.00716(17)
O84	1	0.19706(5)	0.73903(10)	0.1079(2)	0.0077(3)
	1	0.19719(5)	0.73892(11)	0.1079(2)	0.0076(4)
	1	0.19725(3)	0.73883(5)	0.10820(12)	0.00724(16)
O85	1	0.27199(5)	0.33432(10)	0.1092(2)	0.0076(3)
	1	0.27211(5)	0.33443(11)	0.1093(2)	0.0070(4)
	1	0.27232(3)	0.33434(6)	0.10981(12)	0.00912(18)
O86	1	0.03184(5)	0.42535(10)	0.1085(2)	0.0072(3)
	1	0.03206(5)	0.42537(11)	0.1084(2)	0.0070(4)
	1	0.03188(3)	0.42529(6)	0.10978(12)	0.00850(18)
O87	1	0.86374(5)	0.73899(11)	0.7747(2)	0.0078(4)
	1	0.86386(5)	0.73892(11)	0.7746(2)	0.0076(4)
	1	0.86405(3)	0.73764(6)	0.77570(12)	0.00769(17)
O88	1	0.93863(5)	0.33438(11)	0.7759(2)	0.0072(4)
	1	0.93879(5)	0.33449(11)	0.7759(2)	0.0070(4)
	1	0.93903(3)	0.33350(5)	0.77891(12)	0.00655(14)
O89	1	0.69849(5)	0.42539(10)	0.7752(2)	0.0073(3)
	1	0.69873(5)	0.42537(11)	0.7751(2)	0.0067(4)
	1	0.69867(3)	0.42547(5)	0.77620(12)	0.00613(13)

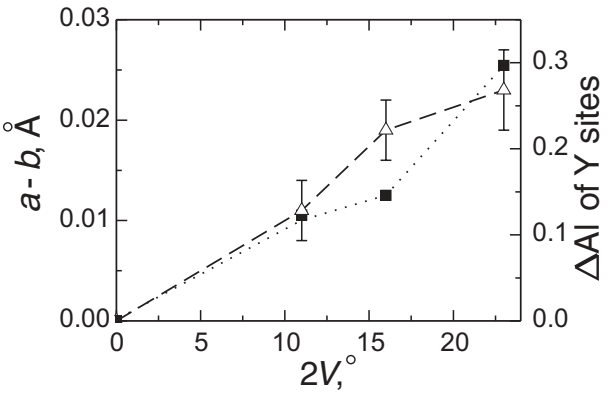

FIGURE 7. The difference between the lattice constants *a* and *b* (triangles) and the mean difference of the Al concentrations in the Y octahedra in the monoclinic approximation, $\Delta Al = x_{Y3} - (x_{Y1} + x_{Y2})/2$, (squares) vs. axial angle $2V$. Lines are guides to the eye.

TABLE 6. Occupancies, fractional atomic coordinates and equivalent displacement parameters for the samples S1 (upper line), S6 (middle line), and S5 (lower line) with e.s.d.s in parentheses in space group *R*1*

Site	Composition/ Site occupancy	*x*	*y*	*z*	U_{eq}, Å^2
X	$Na_{0.31(1)}Ca_{0.69(1)}$	0	0	0.23724(10)	0.01543(19)
	$Na_{0.30(1)}Ca_{0.70(1)}$	0	0	0.23736(11)	0.0165(2)
	$Na_{0.47(1)}Ca_{0.53(1)}$	0	0	0.23734(13)	0.0108(2)
Y1	$Al_{0.572(5)}Li_{0.428(5)}$	0.12508(8)	0.06264(7)	0.63408(15)	0.0072(3)
	$Al_{0.587(6)}Li_{0.413(6)}$	0.12527(8)	0.06264(8)	0.63388(16)	0.0076(3)
	$Al_{0.629(6)}Li_{0.371(6)}$	0.12648(9)	0.06322(9)	0.63391(18)	0.0064(3)
Y2	$Al_{0.436(5)}Li_{0.564(5)}$	0.93855(10)	0.06204(9)	0.63349(18)	0.0097(4)
	$Al_{0.426(6)}Li_{0.574(6)}$	0.93865(10)	0.06199(11)	0.6335(2)	0.0102(4)
	$Al_{0.339(6)}Li_{0.661(6)}$	0.93888(13)	0.06221(13)	0.6333(3)	0.0074(5)
Y3	$Al_{0.464(5)}Li_{0.536(5)}$	0.93842(9)	0.87634(9)	0.63378(18)	0.0095(4)
	$Al_{0.478(6)}Li_{0.522(6)}$	0.93856(10)	0.87639(10)	0.6336(2)	0.0106(4)
	$Al_{0.350(6)}Li_{0.650(6)}$	0.93900(13)	0.87681(13)	0.6332(3)	0.0078(5)
Z1	$Al_{1.0}$	0.29802(6)	0.26085(6)	0.61144(11)	0.00563(10)
	$Al_{1.0}$	0.29821(6)	0.26094(6)	0.61135(11)	0.00546(11)
	$Al_{1.0}$	0.29934(7)	0.26196(7)	0.61113(13)	0.00588(12)
Z2	$Al_{1.0}$	0.74136(6)	0.03789(5)	0.61101(11)	0.00550(10)
	$Al_{1.0}$	0.74160(6)	0.03797(6)	0.61098(11)	0.00549(11)
	$Al_{1.0}$	0.74240(7)	0.03855(7)	0.61054(14)	0.00577(12)
Z3	$Al_{1.0}$	0.96367(6)	0.70413(6)	0.61101(10)	0.00562(10)
	$Al_{1.0}$	0.96382(6)	0.70418(6)	0.61093(12)	0.00556(11)
	$Al_{1.0}$	0.96444(7)	0.70504(7)	0.61037(13)	0.00582(12)
Z4	$Al_{1.0}$	0.74117(6)	0.70330(6)	0.61116(10)	0.00550(10)
	$Al_{1.0}$	0.74127(6)	0.70329(6)	0.61101(12)	0.00545(11)
	$Al_{1.0}$	0.74230(7)	0.70352(7)	0.61064(13)	0.00569(12)
Z5	$Al_{1.0}$	0.29793(6)	0.03715(5)	0.61138(11)	0.00571(10)
	$Al_{1.0}$	0.29805(6)	0.03713(6)	0.61137(12)	0.00556(12)
	$Al_{1.0}$	0.29924(7)	0.03713(7)	0.61112(13)	0.00568(12)
Z6	$Al_{1.0}$	0.96356(6)	0.25936(6)	0.61100(11)	0.00563(10)
	$Al_{1.0}$	0.96364(6)	0.25928(6)	0.61085(11)	0.00555(12)
	$Al_{1.0}$	0.96450(7)	0.25920(7)	0.61042(13)	0.00597(12)
B1	1	0.11029(16)	0.21846(15)	0.4543(3)	0.0058(3)
	1	0.11051(17)	0.21844(17)	0.4539(3)	0.0058(3)
	1	0.11137(19)	0.2188(2)	0.4539(4)	0.0064(4)
B2	1	0.78296(16)	0.89139(14)	0.4536(3)	0.0060(3)
	1	0.78329 (17)	0.89142(17)	0.4535(3)	0.0059(3)
	1	0.78386(19)	0.89179(19)	0.4531(4)	0.0061(4)
B3	1	0.11012(16)	0.89164(14)	0.4545(3)	0.0059(3)
	1	0.11026(17)	0.89188(17)	0.4543(3)	0.0060(3)
	1	0.11152(19)	0.89251(19)	0.4543(4)	0.0060(4)
T1	$Si_{0.97(1)}B_{0.03(1)}$	0.19296(6)	0.19063(5)	0	0.00384(16)
	$Si_{0.98(1)}B_{0.02(1)}$	0.19313(6)	0.19070(6)	0	0.00403(18)
	$Si_{0.97(1)}B_{0.03(1)}$	0.19393(7)	0.19104(7)	0	0.00414(17)
T2	$Si_{0.97(1)}B_{0.03(1)}$	0.81041(6)	0.00228(5)	–0.00111(10)	0.00384(16)
	$Si_{1.00(1)}$	0.81054(6)	0.00231(6)	–0.00123(11)	0.00453(18)
	$Si_{0.96(1)}B_{0.04(1)}$	0.81114(7)	0.00260(7)	–0.00180(13)	0.00416(18)
T3	$Si_{0.96(1)}B_{0.04(1)}$	0.99872(6)	0.80850(5)	–0.00073(10)	0.00393(16)
	$Si_{0.95(1)}B_{0.05(1)}$	0.99885(6)	0.80855(6)	–0.00080(11)	0.00362(18)
	$Si_{0.94(1)}B_{0.06(1)}$	0.99960(7)	0.80913(7)	–0.00168(13)	0.00392(18)
T4	$Si_{0.97(1)}B_{0.03(1)}$	0.81037(6)	0.80806(5)	–0.00085(9)	0.00395(16)
	$Si_{0.96(1)}B_{0.04(1)}$	0.81046(6)	0.80804(6)	–0.00090(11)	0.00360(18)
	$Si_{0.96(1)}B_{0.04(1)}$	0.81109(7)	0.80831(7)	–0.00179(12)	0.00389(17)
T5	$Si_{0.98(1)}B_{0.02(1)}$	0.19287(6)	0.00232(5)	0.00005(10)	0.00412(16)
	$Si_{0.97(1)}B_{0.03(1)}$	0.19302(6)	0.00239(6)	0.00001(10)	0.00363(18)
	$Si_{0.96(1)}B_{0.04(1)}$	0.19391(7)	0.00275(7)	0.00008(13)	0.00392(17)
T6	$Si_{0.96(1)}B_{0.04(1)}$	0.99873(6)	0.19022(5)	–0.00100(10)	0.00385(16)
	$Si_{0.98(1)}B_{0.02(1)}$	0.99886(6)	0.19021(6)	–0.00108(10)	0.00429(18)
	$Si_{0.94(1)}B_{0.06(1)}$	0.99961(7)	0.19029(7)	–0.00184(12)	0.00379(17)
O1W	$F_{1.05(1)}$	0	0	0.7879(3)	0.0559(9)
	$F_{1.08(1)}$	0	0	0.7874(3)	0.0573(9)
	$F_{1.02(1)}$	0	0	0.7879(4)	0.0561(12)
O21	1	0.06269(15)	0.11992(11)	0.4807(2)	0.0167(3)
	1	0.06327(13)	0.12005(15)	0.4808(3)	0.0163(3)
	1	0.06583(17)	0.12040(15)	0.4813(3)	0.0163(4)
O22	1	0.88106(13)	0.94009(13)	0.4777(3)	0.0158(3)
	1	0.88108(15)	0.93987(15)	0.4782(3)	0.0155(3)
	1	0.88189(15)	0.94070(17)	0.4757(3)	0.0150(4)
O23	1	0.06243(15)	0.94251(14)	0.4808(2)	0.0167(3)
	1	0.06250(15)	0.94245(13)	0.4814(3)	0.0167(3)
	1	0.06578(18)	0.94516(18)	0.4811(3)	0.0162(4)
O31	1	0.26810(13)	0.13407(11)	0.5096(2)	0.0102(3)
	1	0.26790(12)	0.13390(12)	0.5098(2)	0.0101(3)
	1	0.26767(15)	0.13368(14)	0.5092(3)	0.0101(3)
O32	1	0.86551(12)	0.13534(11)	0.5088(2)	0.0101(3)
	1	0.86555(12)	0.13532(14)	0.5086(2)	0.0105(3)
	1	0.86596(14)	0.13607(14)	0.5078(3)	0.0106(3)
O33	1	0.86567(12)	0.73066(12)	0.5089(2)	0.0102(3)
	1	0.86608(14)	0.73086(12)	0.5089(2)	0.0104(3)
	1	0.86577(14)	0.72993(16)	0.5078(3)	0.0100(3)
O41	1	0.09303(11)	0.18469(11)	0.0743(2)	0.0081(2)
	1	0.09302(12)	0.18462(11)	0.0742(2)	0.0080(3)
	1	0.09372(13)	0.18450(14)	0.0741(3)	0.0083(3)
O42	1	0.81547(12)	0.90778(10)	0.0739(2)	0.0084(2)
	1	0.81554(11)	0.90772(11)	0.0737(2)	0.0083(3)
	1	0.81581(14)	0.90771(14)	0.0732(3)	0.0082(3)
O43	1	0.09281(11)	0.90839(10)	0.0747(2)	0.0082(2)
	1	0.09286(12)	0.90842(12)	0.0746(2)	0.0082(3)
	1	0.09364(13)	0.90907(13)	0.0740(3)	0.0083(3)
O51	1	0.18576(12)	0.09287(11)	0.0964(2)	0.0081(2)
	1	0.18597(12)	0.09300(12)	0.0965(2)	0.0083(3)
	1	0.18743(15)	0.09374(14)	0.0960(3)	0.0087(3)
O52	1	0.90897(11)	0.09211(10)	0.0950(2)	0.0083(2)
	1	0.90911(12)	0.09206(13)	0.0947(2)	0.0083(3)
	1	0.91004(14)	0.09213(14)	0.0942(3)	0.0084(3)
O53	1	0.90876(11)	0.81664(11)	0.0955(2)	0.0085(2)
	1	0.90890(13)	0.81665(12)	0.0954(2)	0.0085(3)
	1	0.91001(14)	0.81760(15)	0.0943(3)	0.0087(3)
O61	1	0.19663(11)	0.18599(10)	0.7756(2)	0.0074(2)
	1	0.19672(12)	0.18597 (12)	0.7755(2)	0.0073(3)
	1	0.19744(13)	0.18576(13)	0.7752(3)	0.0073(3)
O62	1	0.81406(11)	0.01001(11)	0.7752(2)	0.0076(2)
	1	0.81422(12)	0.01005(12)	0.7754(2)	0.0075(3)
	1	0.81449(13)	0.01048(14)	0.7749(3)	0.0076(3)
O63	1	0.99138(12)	0.80479(10)	0.7755(2)	0.0075(2)
	1	0.99148(12)	0.80497(12)	0.7753(2)	0.0075(3)
	1	0.99276(14)	0.80547(14)	0.7752(3)	0.0079(3)
O64	1	0.81408(11)	0.80393(10)	0.7755(2)	0.0076(2)
	1	0.81431(12)	0.80401(12)	0.7753(2)	0.0075(3)
	1	0.81444(13)	0.80388(14)	0.7752(3)	0.0080(3)

* The space group *R*1 was constructed using pseudohexagonal triclinic cell and adding (1/3, 2/3, 2/3) and (2/3, 1/3, 1/3) translational equivalents to each of the atoms in the asymmetric unit.

TABLE 6. —*Continued*

Site	Composition/ Site occupancy	*x*	*y*	*z*	U_{eq}, Å^2
O65	1	0.19654(11)	0.01054(11)	0.7756(2)	0.0073(2)
	1	0.19650(12)	0.01058(12)	0.7753(2)	0.0074(3)
	1	0.19724(13)	0.01131(14)	0.7753(3)	0.0074(3)
O66	1	0.99147(12)	0.18670(10)	0.7755(2)	0.0075(2)
	1	0.99170(12)	0.18678(12)	0.7755(2)	0.0073(3)
	1	0.99283(14)	0.18715(14)	0.7751(3)	0.0080(3)
O71	1	0.28671(11)	0.28615(10)	0.0806(2)	0.0065(2)
	1	0.28685(11)	0.28618(12)	0.0807(2)	0.0063(2)
	1	0.28738(13)	0.28683(13)	0.0802(3)	0.0069(3)
O72	1	0.71562(11)	0.00128(10)	0.0810(2)	0.0065(2)
	1	0.71573(12)	0.00131(12)	0.0808(2)	0.0064(3)
	1	0.71632(13)	0.00160(14)	0.0806(2)	0.0065(3)
O73	1	–0.00006(11)	0.71439(10)	0.0812(2)	0.0063(2)
	1	0.00003(12)	0.71439(11)	0.0810(2)	0.0063(2)
	1	0.00068(13)	0.71488(14)	0.0810(2)	0.0067(3)
O74	1	0.71541(11)	0.71427(10)	0.0809(2)	0.0065(2)
	1	0.71551(12)	0.71422(12)	0.0808(2)	0.0063(2)
	1	0.71626(13)	0.71448(13)	0.0805(2)	0.0066(3)
O75	1	0.28662(11)	0.00052(10)	0.0806(2)	0.0064(2)
	1	0.28679(11)	0.00060(11)	0.0805(2)	0.0064(2)
	1	0.28737(13)	0.00043(14)	0.0799(3)	0.0068(3)
O76	1	–0.00011(11)	0.28543(10)	0.0812(2)	0.0064(2)
	1	0.00007(11)	0.28549(12)	0.0809(2)	0.0062(2)
	1	0.00061(13)	0.28545(13)	0.0811(3)	0.0065(3)
O81	1	0.21085(11)	0.27106(11)	0.4415(2)	0.0071(2)
	1	0.21110(12)	0.27111(12)	0.4414(2)	0.0070(3)
	1	0.21233(13)	0.27226(14)	0.4417(3)	0.0077(3)
O82	1	0.73080(11)	0.93991(10)	0.4408(2)	0.0072(2)
	1	0.73099(12)	0.93997(12)	0.4406(2)	0.0071(3)
	1	0.73102(14)	0.94001(14)	0.4406(3)	0.0074(3)
O83	1	0.06089(11)	0.79145(10)	0.4403(2)	0.0077(2)
	1	0.06109(12)	0.79156(12)	0.4403(2)	0.0077(3)
	1	0.06177(14)	0.79258(14)	0.4394(3)	0.0079(3)
O84	1	0.73040(11)	0.79055(10)	0.4410(2)	0.0070(2)
	1	0.73060(12)	0.79052(12)	0.4411(2)	0.0072(3)
	1	0.73104(14)	0.79088(14)	0.4405(3)	0.0077(3)
O85	1	0.21066(11)	0.93980(10)	0.4414(2)	0.0074(2)
	1	0.21081(12)	0.93985(12)	0.4415(2)	0.0072(3)
	1	0.21215(13)	0.93989(14)	0.4419(3)	0.0077(3)
O86	1	0.06087(11)	0.26930(11)	0.4402(2)	0.0076(2)
	1	0.06103(12)	0.26924(12)	0.4400(2)	0.0076(3)
	1	0.06179(14)	0.26900(14)	0.4391(3)	0.0078(3)

* The space group *R*1 was constructed using pseudohexagonal triclinic cell and adding (1/3, 2/3, 2/3) and (2/3, 1/3, 1/3) translational equivalents to each of the atoms in the asymmetric unit.

crystal structure could be considered monoclinic. This monoclinic approximation agrees with the analysis of the intensities of the equivalent reflections (Fig. 4) and seems to be justified. However, a more detailed analysis shows that the site Y2 *always* contains less Al than site Y3 (Tables 5–6, Fig. 6). For the samples S1, S6, and S5, the differences are equal to 0.028, 0.052, and 0.011, corresponding to 5, 9, and 2 e.s.d.s, respectively. The differences in occupancies also correlate with the mean Y-O bond lengths (Tables 6–7, Fig. 6), so that for the samples S1 and S6 the best fitting model corresponds to triclinic symmetry. For the sample S5, however, differences in occupancies are too small to be unambiguously confirmed and formally the symmetry should

TABLE 7. Cation-oxygen bond lengths (Å) in Y octahedra for the tourmaline crystal structures refined in *R*3*m*, *Cm*, and *R*1

	Sample S1	Sample S6	Sample S5
Space group *R*3*m*			
Y – O6 × 2	1.9849(18)	1.9835(19)	1.9787(16)
– O2 × 2	1.9963(18)	1.9961(19)	1.9986(16)
– O1W	2.0270(32)	2.0222(33)	2.0213(27)
– O3	2.1797(27)	2.1710(30)	2.1785(27)
<Y-O>	2.028(31)	2.025(30)	2.026(31)
Space group *Cm*			
Y11 – O21 × 2	1.9722(20)	1.9673(20)	1.9477(11)
– O62 × 2	1.9750(17)	1.9727(19)	1.9710(10)
– O11W	2.0348(19)	2.0369(19)	2.0449(14)
– O31	2.1552(25)	2.1471(26)	2.1269(15)
<Y11-O>	2.014(30)	2.011(29)	2.002(29)
Y12 – O23 × 2	1.9714(20)	1.9678(21)	1.9482(12)
– O65 × 2	1.9772(18)	1.9727(19)	1.9656(11)
– O12W	1.9990(41)	2.0016(40)	1.8797(19)
– O33	2.1539(26)	2.1475(26)	2.1421(14)
<Y12-O>	2.008(29)	2.005(29)	1.975(36)
Y13 – O25 × 2	1.9735(21)	1.9691(21)	1.9434(11)
– O68 × 2	1.9751(19)	1.9732(19)	1.9597(10)
– O13W	1.9986(41)	2.0003(38)	1.8933(21)
– O35	2.1524(27)	2.1485(26)	2.1265(16)
<Y13-O>	2.008(29)	2.006(29)	1.971(33)
Y21 – O61	1.9889(20)	1.9879(21)	2.0063(12)
– O63	1.9901(18)	1.9896(19)	1.9945(12)
– O22	2.0033(20)	1.9995(21)	2.0006(14)
– O21	2.0252(20)	2.0231(21)	2.0563(13)
– O11W	2.0209(18)	2.0155(18)	2.0152(15)
– O32	2.1899(20)	2.1903(22)	2.2044(13)
<Y21-O>	2.036(31)	2.034(32)	2.046(33)
Y22 – O64	1.9894(20)	1.9873(21)	1.9782(12)
– O66	1.9912(19)	1.9898(19)	1.9902(12)
– O24	2.0039(20)	1.9999(21)	2.0156(12)
– O23	2.0234(21)	2.0226(21)	2.0661(13)
– O12W	2.0370(27)	2.0357(27)	2.0958(15)
– O34	2.1911(21)	2.1897(22)	2.2136(13)
<Y22-O>	2.039(31)	2.038(31)	2.060(36)
Y23 – O67	1.9880(21)	1.9878(22)	1.9875(12)
– O69	1.9896(19)	1.9895(20)	1.9973(12)
– O26	2.0025(20)	2.0004(21)	2.0083(12)
– O25	2.0240(21)	2.0216(22)	2.0354(13)
– O13W	2.0402(28)	2.0359(27)	2.1127(16)
– O36	2.1894(22)	2.1891(22)	2.1907(12)
<Y23-O>	2.039(31)	2.037(31)	2.055(33)
Space group *R*1			
Y1 – O21	1.9708(20)	1.9668(22)	1.9445(25)
– O65	1.9768(16)	1.9734(18)	1.9633(20)
– O61	1.9761(16)	1.9774(18)	1.9633(20)
– O1W	2.0366(16)	2.0350(16)	2.0538(18)
– O23	1.9770(20)	1.9763(22)	1.9492(25)
– O31	2.1545(21)	2.1459(20)	2.1327(23)
<Y1-O>	2.015(30)	2.012(29)	2.001(31)
Y2 – O62	1.9915(20)	1.9887(20)	1.9904(24)
– O66	1.9925(17)	1.9954(20)	1.9920(24)
– O22	2.0081(21)	2.0098(23)	2.0079(27)
– O1W	2.0182(17)	2.0145(19)	2.0151(23)
– O21	2.0228(24)	2.0256(23)	2.0534(28)
– O32	2.1944(20)	2.1964(23)	2.1995(28)
<Y2-O>	2.038(32)	2.038(32)	2.043(33)
Y3 – O63	1.9880(17)	1.9865(19)	1.9931(24)
– O64	1.9895(20)	1.9861(19)	1.9940(24)
– O22	1.9979(20)	1.9941(22)	2.0003(27)
– O1W	2.0206(17)	2.0200(18)	2.0152(23)
– O23	2.0218(24)	2.0160(23)	2.0516(28)
– O33	2.1881(20)	2.1875(22)	2.2025(28)
<Y3-O>	2.034(31)	2.032(32)	2.043(33)

Note: The e.s.d.s for the mean values <Y-O> are calculated from the scatter of the individual bond lengths.

be considered as monoclinic. We believe that the symmetry of this sample is nevertheless triclinic but with a very small deviation from monoclinic.

Thus, the crystal symmetry should be basically considered as monoclinic with different degrees of triclinic distortions. To characterize the degree of triclinic distortions, we introduce the value $\xi = (x_{Y1} - x_{Y2})/(x_{Y3} - x_{Y2})$, which is close to 0 for monoclinic symmetry and is about 1 for the triclinic crystal structure without any pseudomonoclinicity. This value is equal to 0.20, 0.37, and 0.04 for the samples S1, S6, and S5, respectively, suggesting significant triclinic distortions for the samples S1 and S6 and slight or even negligible distortions for sample S5. A similar symmetry variability was observed for isomorphous series of ugrandite garnets (Wildner and Andrut 2001; Shtukenberg et al. 2005) and sodium chlorate-bromate (Shtukenberg et al. 2004).

In the refined structures, the Z sites are fully occupied by Al^{3+}, and the mean cation-oxygen bond lengths <Z-O> ranges only from 1.903 to 1.907 Å for the three samples (Table 8). Hence, the <Z-O> distances are essentially the same and consistent with the mean <Z-O> bond lengths reported for five elbaite-liddicoatite tourmalines with Z sites fully occupied by Al and Y sites nearly fully occupied by Al and Li (Nuber and Schmetzer 1981; Burns et al. 1994; MacDonald and Hawthorne 1995; Rozhdestvenskaya et al. 2005). The same applies to the mean <T–O> and <B-O> bond lengths: 1.615–1.620 and 1.372–1.380 Å, respectively (Table 8) as compared to 1.616–1.621 and 1.370–1.379 Å reported by the above authors. Only the <X-O> vary between 2.623–2.633 Å (Table 8) and are thus somewhat shorter than the reported 2.645–2.675 Å. This suggests minor amount of vacancies at X sites in our samples (0.07–0.13 apfu (Table 2) compared with 0.26–0.44 apfu in four from five samples, whose crystal structures were refined in the above mentioned papers; amount of vacancies in the fifth sample is only 0.01 apfu, and it is characterized by the minimal <X-O> distance equal to 2.645 Å).

The <T-O> bond lengths observed are somewhat shorter than the typical Si-O bond length. The possible explanation is partial occupancy of the T sites by B that was found in several papers (Hughes et al. 2000; Schreyer et al. 2002; Marshall et al. 2004; Ertl et al. 2005). Indeed, refinement of corresponding occupancies (Tables 4–6) argues for a minor (up to 0.06 apfu) admixture of B at the T sites in all samples studied.

TABLE 8. Selected mean bond lengths (Å) with e.s.d.s calculated from the scatter of the individual bond lengths for the tourmaline crystal structures refined in *R*3*m*, *Cm*, and *R*1

	Space group	Sample S1	Sample S6	Sample S5
<X-O>	*R*3*m*	2.628(123)	2.624(127)	2.623(128)
	Cm	2.629(63)–2.630(63)	1.629(63)	2.624(61)–2.633(65)
	*R*1	2.629(63)	2.629(63)	2.627(63)
<Z-O>	*R*3*m*	1.906(17)	1.903(17)	1.904(17)
	Cm	1.905(18)	1.905(16)–1.906(18)	1.904(16)–1.907(19)
	*R*1	1.906(18)–1.907(17)	1.905(16)–1.907(18)	1.904(18)–1.905(19)
<B-O>	*R*3*m*	1.375(6)	1.376(7)	1.377(4)
	Cm	1.375(6–1.377(10)	1.376(5)–1.377(9)	1.372(3)–1.380(6)
	*R*1	1.376(6)–1.377(10)	1.376(6)–1.376(12)	1.374(7)–1.377(11)
<T-O>	*R*3*m*	1.620(11)	1.618(11)	1.617(11)
	Cm	1.617(10)–1.619(12)	1.617(10)–1.619(12)	1.615(9)–1.620(15)
	*R*1	1.618(12)–1.620(10)	1.618(12)–1.620(10)	1.617(13)–1.618(12)

Note: The ranges given for the mean bond lengths <Z-O>, <B-O>, and <T-O> (space group *R*1) indicate that the individual ZO_6, BO_3, and TO_4 coordination polyhedra remain essentially unaffected by the symmetry reduction.

DISCUSSION

The growth ordering of the Li and Al atoms results from the reduction of the bulk crystal symmetry to that of the growth front (i.e., to the symmetry of a face or of a step in the cases of normal or tangential growth, respectively). The $\{02\bar{2}1\}$ tourmaline faces have the point group symmetry *m*, and steps on these faces have the symmetry 1 (or *m* if the step is perpendicular to the mirror plane in the trigonal crystal structure). This means that the dissymmetrization should lead either to monoclinic symmetry when the crystal grows by normal mechanism or to triclinic when it grows by step motion on the face. In the first case, the three initially equivalent Y octahedra are divided into two groups: Y1 located on the mirror plane, and Y2 and Y3, linked by a mirror plane and having equal occupancies. In the second case, all three Y octahedra of the same triad are non-equivalent and can have different occupancies. However, due to the preservation of the *R*-lattice actually only two different occupancies are to be considered for *Cm* (rather than six as allowed by *Cm*) and likewise only three for *R*1 (rather than nine as allowed by *P*1). This is because in *R*3*m*, the triads of the Y octahedra are related by translation symmetry and therefore have to be equally occupied, even in the course of growth dissymmetrization (Bulka et al. 1980). It is exactly this result that has been experimentally observed.

Finally, one can compare the distribution of the site occupancies with the atomic structure of the growth front. Figure 8 shows a projection of the tourmaline crystal structure onto the $(20\bar{2}1)$ face. With respect to this growth face the Y2 and Y3 octahedra possess the same orientations and environments. The orientation and surroundings of the remaining Y1 octahedron differs from those of Y2 and Y3 so that a basis for an ordered distribution of the cations over the two types of Y sites is established. With respect to any growth step on the $(20\bar{2}1)$ faces (which is not parallel to the $[\bar{1}2\bar{1}0]$ direction), all three types of octahedra Y1,

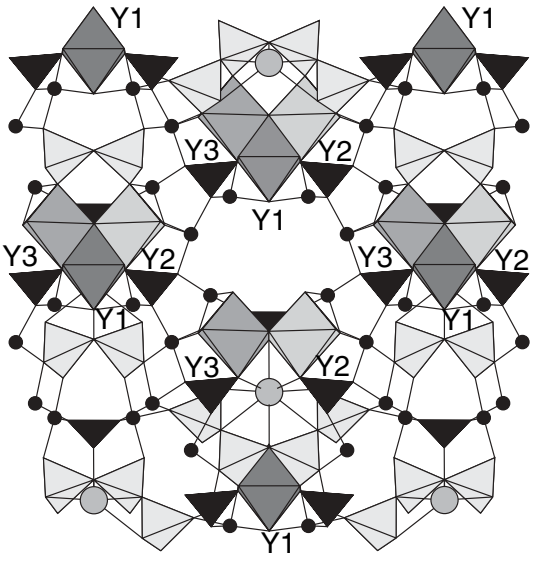

FIGURE 8. Projection of the tourmaline crystal structure on the $(20\bar{2}1)$ growth face, ($[\bar{1}2\bar{1}0]$ horizontal). Light gray tetrahedra denote SiO_4 groups, black triangles BO_3 groups, gray circles X (Na, Ca) sites, and black circles Z (Al) sites. Variation in Y-site occupancy is shown by different gray levels.

Y2, and Y3, are different and allow for three different occupancies. Like other minerals of pegmatite veins, tourmaline crystals are formed by tangential growth due to step motion along the crystal face. Since this can explain the triclinic symmetry and the different occupancies of the three Y octahedra, the growth dissymmetrization hypothesis correctly predicts the crystal symmetry and the relative distribution of occupancies.

As seen from Figure 7, differences in the lattice constants, $a - b$, as well as the differences in the occupancies of the Y sites, $\Delta Al = x_{Y1} - (x_{Y2} + x_{Y3})/2$, correlate with the axial angle $2V$. This suggests that the cation ordering is the main reason for the anomalous biaxiality of the tourmaline samples studied. Certainly, other reasons for optical anomalies such as internal stress can also affect the observed optical pattern; however, such contributions are not expected to be significant. On the other hand, an internal stress originating from the zoning and sector zoning compositional inhomogeneities might be a reason for the variation of the optic axial plane orientations within the growth sectors (Fig. 2).

The growth induced ordering found is also supported by the strong increase of the axial angle going from S1 to S5 and S6 (Fig. 3). Since the overall chemical compositions of all samples are nearly the same (Tables 2 and 4), the marked axial angle variations as well as the degrees of Al/Li ordering (Fig. 6) can be ascribed to changes of the growth conditions, e.g., to a decrease of the growth temperature and/or of the growth rate in the late stages of the crystal growth.

Acknowledgments

This work was supported in part by INTAS YS Fellowship program (project 2004-83-2826) and by Russian Foundation for Basic Researches (projects 04-05-64298 and 05-05-64289). The authors thank A. Ertl, E.S. Grew, and anonymous reviewer for their careful reviews of the manuscript.

References cited

Akizuki, M., Kuribayashi, T., Nagase, T., and Kitakaze, A. (2001) Triclinic liddicoatite and elbaite in growth sectors of tourmaline from Madagascar. American Mineralogist, 86, 364–369.

Aurisicchio, C., Demartin, F., Ottolini, L., and Pezzotta, F. (1999) Homogeneous liddicoatite from Madagascar: a posible reference material? First EPMA, SIMS and SREF data. European Journal of Mineralogy, 11, 237–242.

Belov, N.V. (1976) Essays on Structural Mineralogy. Nedra, Moscow (in Russian).

Blessing, R.H. (1995) An empirical correction for absorption anisotropy. Acta Crystallographica, A51, 33–38.

Brauns, R. (1891) Die optischen Anomalien der Kristalle. Bei S. Hirzel, Leipzig.

Bulka, G.R., Vinokurov, V.M., Nizamutdinow, N.M., and Hasanova, N.M. (1980) Dissymmetrization of crystals: theory and experiment. Physics and Chemistry of Minerals, 6, 283–293.

Burns, P.C., MacDonald, J., and Hawthorne, F.C. (1994) The crystal chemistry of manganese-bearing elbaite. Canadian Mineralogist, 32, 31–43.

Ertl, A., Rossman, G.R., Hughes, J.M. Prowatke, S., Ludwig, Th. (2005) Mn-bearing "oxy-rossmanite" with tetrahedrally coordinated Al and B from Austria; structure, chemistry, and infrared and optical spectroscopic study. American Mineralogist, 90, 481–487.

Foord, E.E. and Cunningham, C.G. (1978) Thermal transformation of anomalously biaxial dimetric crystals. American Mineralogist, 63, 747–749.

Foord, E.E. and Mills, B.A. (1978) Biaxiality in "isometric" and "dimetric" crystals. American Mineralogist, 63, 316–325.

Gorskaya, M.G., Frank-Kamenetskaya, O.V., Rozhdestvenskaya, I.V., and Frank-Kamenetskii, V.A. (1982) Refinement of the crystal structure of Al-rich elbaite, and some aspects of the crystal chemistry of tourmalines. Soviet Physics Crystallography, 27(1), 63–66.

Gorskaya, M.G., Punin, Yu.O., Sokolov, P.B., and Krezer, Yu.A. (1992) Compositional inhomogeneity and heterometry in the crystals of polychromic tourmalines. Mineralogical Journal, 14(3), 8–20 (in Russian).

Hawthorne, F.C. and Henry, D.J. (1999) Classification of the minerals of tourmaline group. European Journal of Mineralogy, 11, 201–215.

Hughes, J.M., Ertl, A., Dyar, M.D., Grew, E.S., Shearer, Ch.K., Yates, M.G., and Guidotti, Ch.V. (2000) Tetrahedrally coordinated boron in a tourmaline; boron-rich olenite from Stoffhuette, Koralpe, Austria. Canadian Mineralogist, 38, 861–868.

Kahr, B. and McBride, J.M. (1992) Optical anomalous crystals. Angewandte Chemie, 31, 1–26.

MacDonald, J. and Hawthorne, F.C. (1995) Cu-bearing tourmaline from Paraiba, Brazil. Acta Crystallographica C, 51, 555–557.

Marshall, H.R., Ertl, A., Hughes, J.M., and McCammon, C. (2004) Metamorphic Na- and OH-rich disordered dravite with tetrahedral boron, associated with omphacite, from Syros, Greece; chemistry and structure. European Journal of Mineralogy, 16, 817–823.

Nuber, B. and Schmetzer, K. (1981) Strukturverfeinerung von Liddicoatit. Neues Jahrbuch für Mineralogie. Monatshefte, 1981, 215–219.

Rozhdestvenskaya, I.V., Frank-Kamenetskaya, O.V., Zolotarev, A.A., Bronzova, Yu.M., and Bannova, I.I. (2005) Refinement of the crystal structures of three fluorine-bearing elbaites. Crystallography Reports, 50, 981–988.

Schreyer, W., Hughes, J.M., Bernhardt, H.-J., Kalt, A., Prowatke, S., and Ertl, A. (2002) Reexamination of olenite from the type locality; detection of boron in tetrahedral coordination. European Journal of Mineralogy, 14, 935–942.

Sheldrick, G.M. (1997) SHELX-97. Program for the Solutions and Refinement of Crystal Structures. University of Göttingen, Germany.

Shtukenberg, A.G., Punin, Yu.O., Frank-Kamenetskaya, O.V., Kovalev, O.G., and Sokolov, P.B. (2001) On the origin of anomalous birefringence in grandite garnets. Mineralogical Magazine, 65, 445–459.

Shtukenberg, A.G., Rozhdestvenskaya, I.V., Popov, D.Yu., and Punin, Yu.O. (2004) Kinetic ordering of atoms in sodium chlorate-bromate solid solutions. Journal of Solid State Chemistry, 177, 4732–4742.

Shtukenberg, A.G., Popov, D.Yu., and Punin, Yu.O. (2005) Growth ordering and anomalous birefringence in ugrandite garnets. Mineralogical Magazine, 69, 537–550.

Shtukenberg, A.G., Punin, Yu.O., and Frank-Kamenetskaya, O.V. (2006) Kinetic ordering and the growth dissymmetrisation in crystalline solid solutions. Russian Chemical Reviews, 75, 1212–1236.

Wildner, M. and Andrut, M. (2001) The crystal chemistry of birefringent natural uvarovites: Part II. Single-crystal X-ray structures. American Mineralogist, 86, 1231–1251.

Wilson, A.J.C., Ed. (1992) International Tables for Crystallography Vol. C: Mathematical, Physical and Chemical Tables (1st ed.), 900 p. Kluwer Academic Publishers, Dordrecht.

Manuscript received June 21, 2006
Manuscript accepted November 16, 2006
Manuscript handled by Edward Grew